Energy & Environmental Science

Accepted Manuscript

This article can be cited before page numbers have been issued, to do this please use: Q. Ma, C. Ji, Z. Wang, R. Wang, L. Zhang, H. Li, Y. Xu, Q. Zhang, D. Chao and C. Zhang, *Energy Environ. Sci.*, 2026, DOI: 10.1039/D6EE00199H.

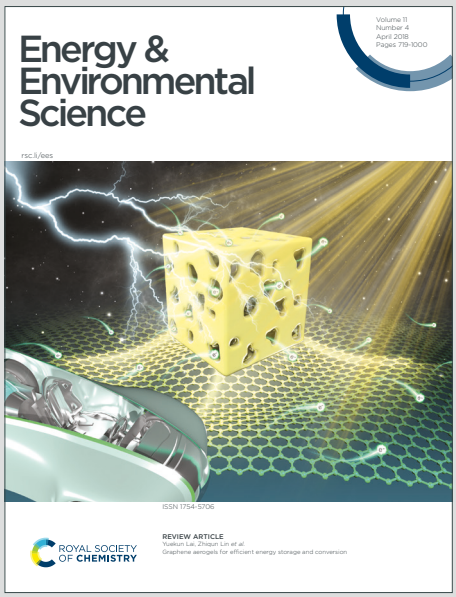

ROYAL SOCIETY OF CHEMISTRY

rsc.li/ees

View Article Online
DOI: 10.1039/D6EE00199H

Broader context

Rechargeable organic cathodes are capturing increasing attention in aqueous Zinc-ion batteries (AZIBs), owing to its high theoretical capacity, sustainability, and structural designability. However, their widespread practical application poses significant challenges, primarily due to insufficient redox activity and compromised electronic conductivity, which collectively curtail energy density and reaction kinetics under demanding operational environments. We have designed PMPZ through molecular engineering, simultaneously addressing the major challenges related to cycling stability, operational temperature range, and energy density. Furthermore, multi-scale structural and electrochemical analyses correlated the designed architecture of PMPZ with its performance, revealing the underpinnings of its redox activity, reaction mechanism, and stability. This work thereby ushers in a paradigm shift from empirical searches to a rational design methodology for organic cathode materials.

View Article Online
DOI: 10.1039/D6EE00199H

ARTICLE

Molecular Engineering of Conjugated Polymer Cathodes via One-Pot Preparation for High-Rate and Ultra-Stable Aqueous/Seawater Zn-Ion Batteries under Harsh Conditions

Received 00th January 20xx,
Accepted 00th January 20xx

DOI: 10.1039/x0xx00000x

Quanwei Ma,‡[a] Cheng Ji,‡[a] Zeyu Wang,[b] Rui Wang,[a] Longhai Zhang,[a] Hongbao Li,[a] Ying Xu,[c] Qianyu Zhang,[d] Dongliang Chao,*[b] and Chaofeng Zhang*[a]

Organic materials are promising candidates for high-performance aqueous Zn-ion batteries (AZIBs) cathodes owing to their high capacity, structural adjustability, and sustainability. However, their practical application is hindered by limited redox activity and low electronic conductivity under harsh operating conditions. Here, we report an organic polymer cathode using a simple one-pot preparation, poly (Mellitic Trianhydride-Phenazine) (PMPZ), featuring a fully conjugated structure and abundant active functional groups. The incorporation of heterocyclic conjugated units into the conjugated structure enhances electron affinity and π-electron delocalization of polymer, resulting in high redox activity and significantly elevated conductivity. Meanwhile, multiple C=O and C=N redox-active centers act cooperatively to enable multielectron redox process through this delocalization pathway, improving the charge storage and reaction kinetics. Through combined theoretical and *operando* synchrotron experimental studies, we further elucidate that this fully conjugated structure facilitates reversible Zn^{2+}/H^{+} co-storage with multiple electron transfer. Consequently, the PMPZ cathode demonstrates exceptional electrochemical performance with remarkable rate capability and outstanding cycling stability across a wide temperature range from −50 to 50 °C, even at seawater-based electrolytes. This work provides a novel design strategy for developing high-performance AZIB cathodes capable of operating under extreme conditions.

Introduction

The increasing global demand for efficient utilization and distribution of renewable energy for power generation has spurred extensive research into advanced energy storage technologies.[1-4] Rechargeable aqueous batteries are promising for grid-scale energy storage, owing to their inherent safety, environmental sustainability, and low cost.[5-10] Among them, aqueous zinc-ion batteries (AZIBs) have garnered significant attention owing to the natural abundance of Zn, eco-friendliness, high theoretical capacity (820 mAh g^{-1}), and favorable redox potential (−0.76 V vs. SHE).[11-15] Cathode materials are critical to achieving high performance in AZIBs. Currently, numerous inorganic cathode materials, such as Mn-based/V-based compounds, and Prussian blue analogues (PBAs), have been widely explored as cathodes in these systems.[16, 17] Nevertheless, the advancement of high-performance AZIBs was hampered by considerable hurdles. The Zn^{2+} ion with a relatively high charge density (charge-to-size ratio) and strong coulombic interactions, severely hinder its diffusion kinetics within the rigid lattice frameworks of these inorganic cathodes.[18, 19] Moreover, the repeated intercalation/deintercalation of Zn^{2+} frequently induce substantial structural stress, leading to irreversible structural degradation, including structure collapse and dissolution of active material.[20, 21] Consequently, these issues lead to rapid capacity fading and diminished electrochemical performance. Therefore, the exploration and development of novel cathode materials exhibiting superior structural stability and ion diffusion kinetics are crucial for high performance AZIBs.

Organic materials offer a promising alternative for AZIB cathodes due to their sustainability, high theoretical capacity, and structural designability.[18, 22, 23] Unlike inorganic electrodes, organic materials operate through ion-coordination mechanisms and involve reversible bond rearrangement, which enhances the structural stability and reaction kinetics of electrode materials.[24-26] However, they also present inherent drawbacks, such as poor intrinsic electronic conductivity, severe

a. Institutes of Physical Science and Information Technology, Leibniz International Joint Research Centre of Materials Sciences of Anhui Province, Key Laboratory of Environment-Friendly Polymeric Materials of Anhui Province, Anhui University, Hefei 230601, China.
Email: cfz@ahu.edu.cn
b. Laboratory of Advanced Materials, Aqueous Battery Center, Shanghai Key Laboratory of Molecular Catalysis and Innovative Materials, Collaborative Innovation Center of Chemistry for Energy Materials, Shanghai Wusong Laboratory of Materials Science, State Key Laboratory of Porous Materials for Separation and Conversion, College of Smart Materials and Future Energy, Fudan University, Shanghai 200433, China;
Email: chaod@fudan.edu.cn
c. School of Materials Science and Engineering, Anhui University, Hefei 230601, China.
d. College of Materials Science and Engineering, Sichuan University, Chengdu 610064, China.
‡ These authors contribute to this work equally.

View Article Online
DOI: 10.1039/D6EE00109H

dissolution of small-molecule active species in aqueous electrolytes, relatively low operating voltages, and insufficient utilization of redox sites, all of which limit their practical applications.[25] To address these bottlenecks, conjugated organic molecules with extended π-electron structure have garnered significant interest as cathode materials due to their high conductivity and structural stability.[27] In such conjugated systems, π-electrons delocalize along the molecular backbone instead of remaining localized on individual atoms, which reduces the energy gap between the highest occupied molecular orbital (HOMO) and the lowest unoccupied molecular orbital (LUMO) levels, thereby facilitating efficient electron transport.[25, 28] Despite remarkable improvements in structural stability and electronic conductivity over small-molecule, π-conjugated polymers still suffer from critical drawbacks, including the introduction of electrochemically inactive linkages and rigid conjugated backbones, which reduce active-site density and impede Zn^{2+} storage.[29, 30] This phenomenon presents a key challenge for AZIBs, achieving both high activity and sufficient electronic conductivity in an organic cathode. Therefore, the development of novel conjugated organic cathodes is crucial for achieving high-performance AZIBs with high-rate and extended cycle life under harsh operating conditions.

Here, we designed and synthesized a novel fully conjugated organic polymer (PMPZ) through a one-step Friedel–Crafts reaction between phenazine (PNZ) and mellitic tri-anhydride (MT) (**Figure 1a**). The PMPZ polymer achieve significantly greater π-electron delocalization along the molecular backbone by integrating heterocyclic conjugated units, which improves electronic conductivity and strengthens electron affinity. Furthermore, multiple C=O and C=N active groups work synergistically within the delocalized electronic structure to facilitate efficient multi-electron transfer processes, enhancing the charge storage capability and ensuring fast reaction kinetics at different temperatures. Consequently, when used as the cathode for AZIBs, the PMPZ cathode delivers a high capacity of 240 mAh g^{-1} at 0.1 A g^{-1}, exceptional rate capability of 179 mAh g^{-1} at 50 A g^{-1}, and outstanding cycling stability of over 60000 cycles. Benefiting from its unique structure, the PMPZ cathode shows remarkable electrochemical performance across a wide temperature range from 50 °C to −50 °C (**Figure 1b,c**). It delivers a high capacity of 260 mAh g^{-1} and 175 mAh g^{-1} at 0.1 A g^{-1} when operated at 50 °C and −50 °C, respectively, and demonstrates exceptional cycling stability over 10,000 cycles at both temperatures. Even in seawater-based electrolyte, the PMPZ cathode exhibits high capacity of 223 mAh g^{-1} at 0.1 A g^{-1} and maintains stable performance over 5000 cycles. This work offers valuable insights for developing organic cathode materials suited to high-performance AZIBs under harsh conditions.

Results and discussion

Synthesis and Characterizations.

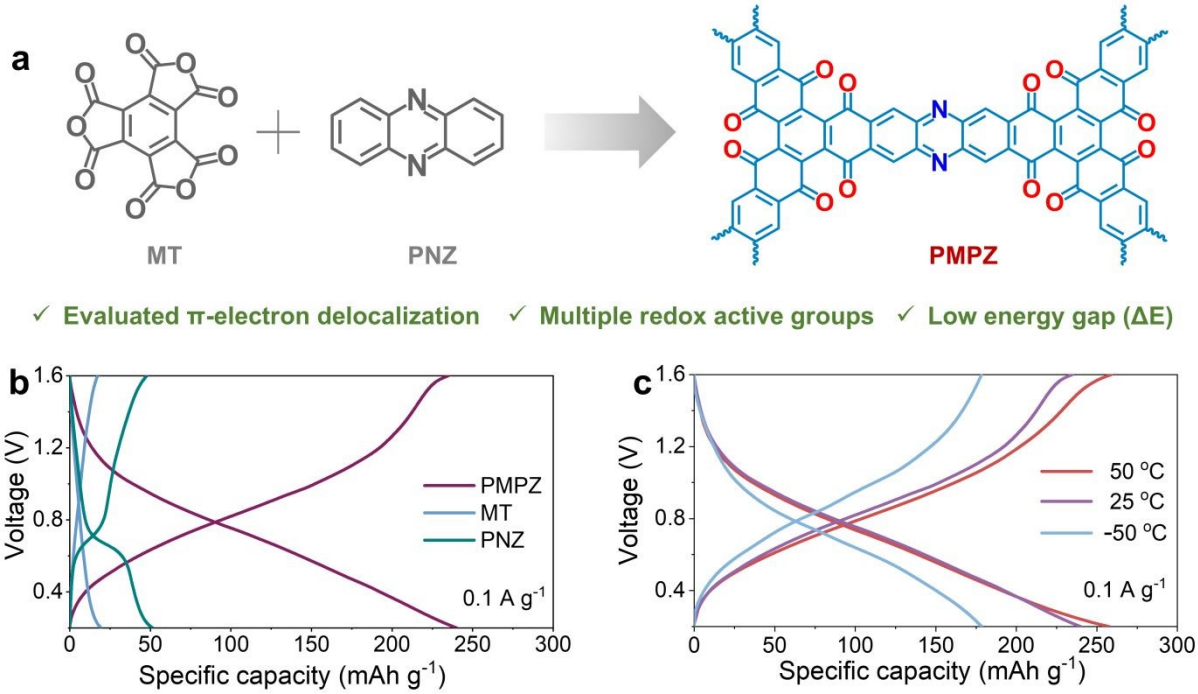

Figure 1. (a) Synthesis diagram of PMPZ. (b) The charge/discharge curves of MT, PNZ, and PMPZ at 0.1 A g^{-1}. (c) The charge/discharge curves of PMPZ at 0.1 A g^{-1} under 50, 25, and −50 °C.

View Article Online
DOI: 10.1039/D5EE04189H

The PMPZ polymer was synthesized by a one-step Friedel–Crafts reaction mechanism between phenazine (PNZ) and mellitic trianhydride (MT) (**Figure 1a**). The chemical structure of as-prepared PMPZ was characterized by Fourier transform infrared (FT-IR), X-ray photoelectron spectroscopy (XPS), and ^{13}C solid-state nuclear magnetic resonance (^{13}C SSNMR) spectroscopy. As depicted in **Figure 2a**, the FT-IR spectrum of PMPZ confirms the presence of C=O and C=N functional groups, as evidenced by the characteristic stretching vibrations at 1675 cm^{-1} and 1542 cm^{-1}, respectively.[27, 31] Additionally, the anhydride bonds at 1850 cm^{-1} disappeared in the FT-IR spectrum of PMPZ compared to that of MT, indicating that the anhydrides bonds were involved in reaction. Moreover, the peaks at 138 and 165 ppm in the ^{13}C SSNMR spectra of PMPZ confirm the presence of C=N and C=O within the molecular structure (**Figure 2b**).[32, 33] Notably, the broad characteristic peaks in the range from110 to 135 ppm of the ^{13}C SSNMR spectra likely arise from overlapping C=C peaks from the aromatic rings of the polymer.[34] XPS analysis of PMPZ confirms that its chemical composition consists primarily of C, N, and O without

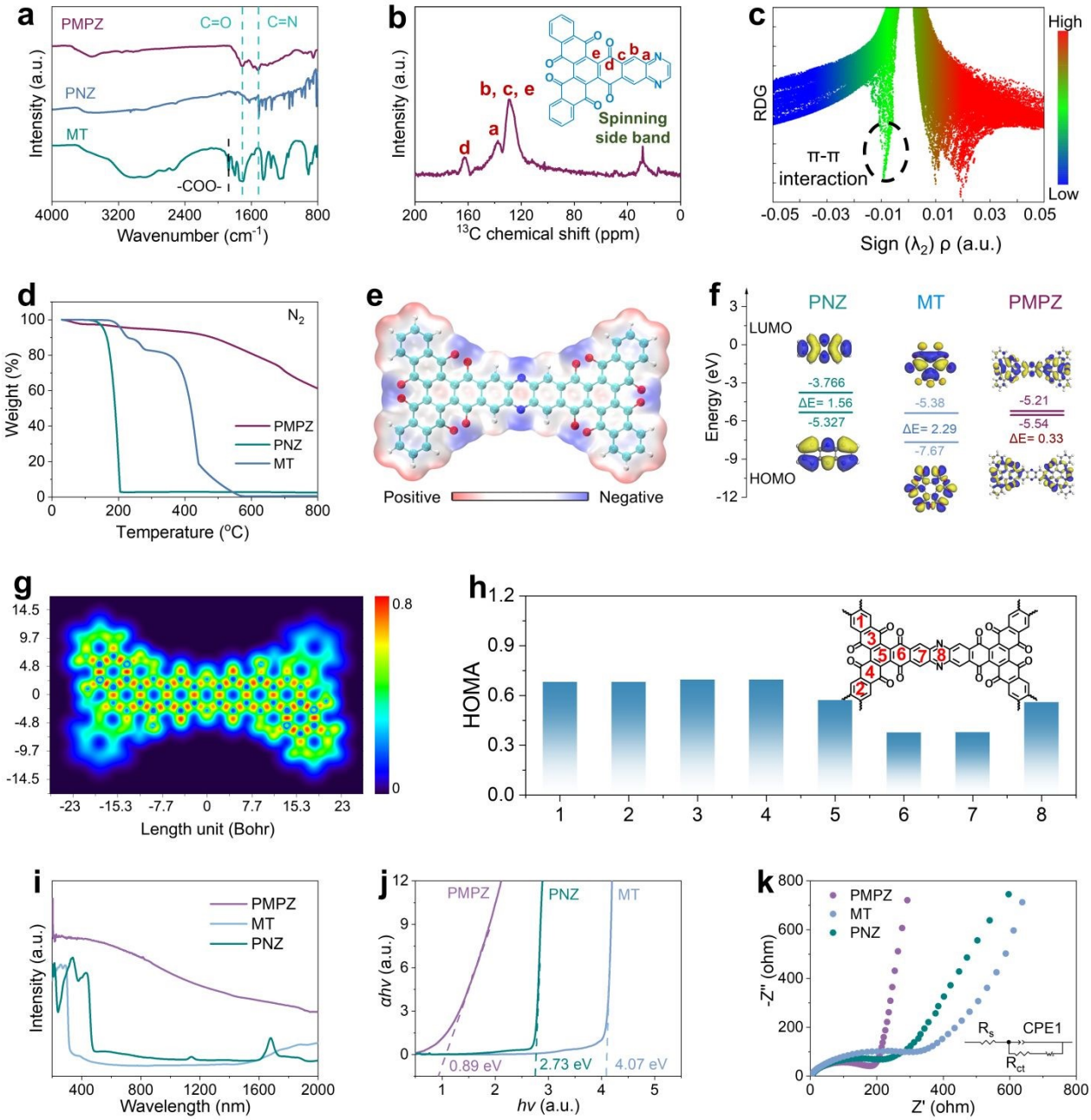

Figure 2. (a) FT-IR spectra of MT, PNZ, and PMPZ. (b) Solid-state ^{13}C NMR spectrum of PMPZ. (c) Plots of reduced density gradient vs. sign(λ_2)ρ for PMPZ. (d) TGA curves of MT, PNZ, and PMPZ under N_2. (e) Optimized geometries and ESP image of PMPZ. (f) Calculated HOMO/LUMO energies of MT, PNZ, and PMPZ. (g) LOL-π image of the PMPZ molecule. (h) Calculated HOMA values of PMPZ. (i) DRUV-vis-NIR spectra of MT, PNZ, and PMPZ. (j) Optical energy gaps of MT, PNZ, and PMPZ. (k) EIS plots of MT, PNZ, and PMPZ (The embedded diagram is an equivalent circuit model).

View Article Online
DOI: 10.1039/D6EE00199H

detectable impurities, as shown in the survey XPS spectrum (**Figure S1a**). The C 1s spectra unambiguously confirms the presence of the C=N (286.3 eV), C=O (288.7 eV), and C-N (285.2 eV) in PMPZ (**Figure S1b**).[18, 35] Consistent with these findings, the deconvoluted N 1s and O 1s spectra (**Figures S1c, d**) exhibit characteristic peaks of C=N, C=O, and C–N species, which corroborates the results in the C1s spectra. Notably, although both the C 1s and O 1s spectra of MT show a dominant C–O peak (**Figure S2**), this feature peak is absent in PMPZ. This result provides direct evidence that the anhydride moiety participated in the reaction, leading to the generation of C=O bonds in PMPZ.

Furthermore, XRD analysis (**Figure S3**) shows a broad peak at approximately 26.1° for the PMPZ polymer, which contrasts with the sharp crystalline peaks of its monomers and indicates π-π stacking between the aromatic units. The non-covalent interactions within the PMPZ polymer were further probed by a reduced density gradient (RDG) analysis, which reveals green spikes in the region where the sign(λ_2)ρ ranges from −0.02 to 0.00 (**Figure 2c**), demonstrating π-π interactions between adjacent polymer molecules.[16, 36, 37] These vertically oriented interactions facilitate highly efficient interfacial charge transfer and enhance redox reaction kinetics in the PMPZ polymer.[38, 39] The thermogravimetric analysis (TGA) curve indicates that PMPZ exhibits excellent thermal stability, with no significant mass loss until the temperature exceeds 400 °C (**Figure 2d**). This exceptional stability arises from strong intramolecular π-π coupling, which delocalizes electronic charges and reduces thermal decomposition reactivity. Consequently, these interactions ensure structural persistence during electrochemical cycling.

As shown in **Figure 2e**, molecular electrostatic potential (ESP) simulations reveal pronounced negative potential regions localized at C=O and C=N groups, illustrating these sites as electrochemically active centers for cation coordination.[40] In addition, the calculated highest occupied molecular orbital (HOMO) and the lowest unoccupied molecular orbital (LUMO) for PMPZ are presented in **Figure 2f**. Frontier molecular orbital analysis shows that the LUMO of PMPZ is **–**5.21 eV, which is significantly lower than conventional organic electrodes (e.g., PNZ: –3.76 eV). This decreased LUMO energy correlates with enhanced electron affinity and a positive shift in reduction potential, confirming superior redox activity. [41, 42] Crucially, PMPZ exhibits an ultranarrow HOMO-LUMO gap of 0.33 eV, substantially reduced versus MT (2.29 eV) and PNZ (1.56 eV), indicating facilitated interorbital electron transitions and intrinsic charge delocalization across the conjugated framework.[27, 28] Moreover, the π-electronic distribution of PMPZ was visualized using the π-electron localized orbital locator (LOL-π) (**Figure 2g**) to analyze the structural stability through the extent of π-conjugation. The LOL-π analysis reveals well-distributed π-electron across the C=C, C=N, and C=O frameworks, revealing an uninterrupted π-conjugation pathway that extends the delocalized range.[31] This enhanced electronic delocalization fundamentally underpins the favorable structural stability of the polymers. Beyond LOL-π analysis, aromaticity serves as a key metric for evaluating the structural stability of organic compounds. As shown in **Figure 2h**, the positive Harmonic Oscillator Model of Aromaticity (HOMA) values for all rings in PMPZ confirm its outstanding aromatic character, indicating enhanced global aromaticity and structural stability, which ensures excellent cycling stability.[43]

Furthermore, diffuse reflectance ultraviolet-visible-near-infrared (DRUV-vis-NIR) spectroscopy reveals that PMPZ exhibits a broad absorption peak centered around 800 nm (**Figure 2i**), which can be attributed to extended conjugation within its polymer backbone. Notably, PMPZ shows a distinctive mid-infrared absorption tail, signifying a more expansive delocalized electronic structure and enhanced intermolecular charge transfer relative to MT and PNZ.[44] Owing to this favourable molecular architecture, PMPZ achieves a narrow optical bandgap of 0.89 eV (**Figure 2j**), significantly lower than that of PNZ (2.73 eV) and MT (4.07 eV). The reduced bandgap endows PMPZ with enhanced electronic conductivity and rapid charge transport capabilities, facilitating high redox reaction kinetics.[17] Moreover, the temperature-dependent electronic conductivity of PMPZ was further investigated (**Figure S4**). The conductivity increases with rising temperature, reaching 2.83×10^{-6} S cm^{-1} at −100 °C, 5.26×10^{-6} S cm^{-1} at room temperature, and 7.25×10^{-6} S cm^{-1} at 100 °C, which guarantees its outstanding electrochemical performance over a wide temperature range. Notably, the electronic conductivity of PPP is far superior to that of most reported organic cathode materials,[45] indicating that such heterocyclic fully conjugated polymers remarkably promote charge transport. After that, electrochemical impedance spectroscopy (EIS) further corroborates these findings, as shown in **Figure 2k**. The EIS plots of PMPZ features a semicircle with a Warburg tail, revealing a significantly lower charge transfer resistance (R_{ct}) of PMPZ (152 Ω) compared to MT (284 Ω) and PNZ (202 Ω). This reduced R_{ct} reflects enhanced electronic conductivity, resulting from the extended conjugated structure, which is consistent with its theoretical calculation results.

The activation energy (E_a) for interfacial charge transfer in the PMPZ cathode was calculated by fitting electrochemical impedance spectroscopy data (**Figure S5**). According to the Arrhenius equation, the ion-storage process in PMPZ exhibits a low E_a value of merely 0.20 eV, which is considerably lower than those of MT (0.25 eV) and PNZ (0.22 eV). Such a reduced activation energy barrier directly verifies that the heteroatom-doped fully conjugated structure effectively enables fast-kinetics charge transfer and redox reactions in the PMPZ cathode. It substantially lowers the reaction energy threshold, allowing ions and charges to readily access and interact with redox-active sites throughout the electrode.[17]

Electrochemical Performance.

The electrochemical performance of PMPZ as an AZIB cathode was evaluated using a coin-type cell with a Zn foil anode and 3M $Zn(ClO_4)_2$ electrolyte. As shown in **Figure 3a**, the cyclic voltammetry (CV) was tested to study the redox reaction behavior of PMPZ at 0.1 mV s^{-1}. The CV curve of PMPZ features two reversible redox couples (0.76/0.71 and 0.52/0.44 V), assigned to the C=O and C=N functional groups, respectively (**Figure S6a**). After the first cycle, the PMPZ cathode shows stable and reversible CV curves, indicating good electrochemical reversibility. Subsequent galvanostatic charge/discharge tests reveal that extended conjugated structure induces extensive π-electron delocalization, leading to an elevated redox potential (**Figures 3b and S6b**).[27] The combination of an

improved voltage plateau and multielectron redox processes collectively boosts increased capacity and energy density. As shown in **Figure 3c and S7a**, the PMPZ cathode displays a high capacity of 240 mAh g^{-1} at 0.1 A g^{-1} and maintains 92.7% of its initial capacity after 100 cycles. In comparison, the MT and PNZ cathodes show low capacity (27 and 82 mAh g^{-1}, respectively) with poor capacity retention (41% for MT and 46% for PNZ), as depicted in **Figures S7b, c**. In addition, when the PMPZ cathode loading is 5 mg cm^{-2}, the PMPZ cathode achieves a discharge capacity of 201 mAh g^{-1} at 0.1 A g^{-1}, and the capacity retention rate is 94% after 100 cycles, which fully verifies that PMPZ can maintain excellent electrochemical performance even under high loading conditions (**Figure 3c and S7d**).

After that, **Figures 3d and S8a** demonstrate the rate performance of PMPZ at different current densities. Specifically, the PMPZ cathode exhibits high specific capacities of 248, 231, 215, 208, 202, 195, 190, 185, and 179 mAh g^{-1} at 0.1, 0.2, 0.5, 1, 2, 5, 10, 20, and 50

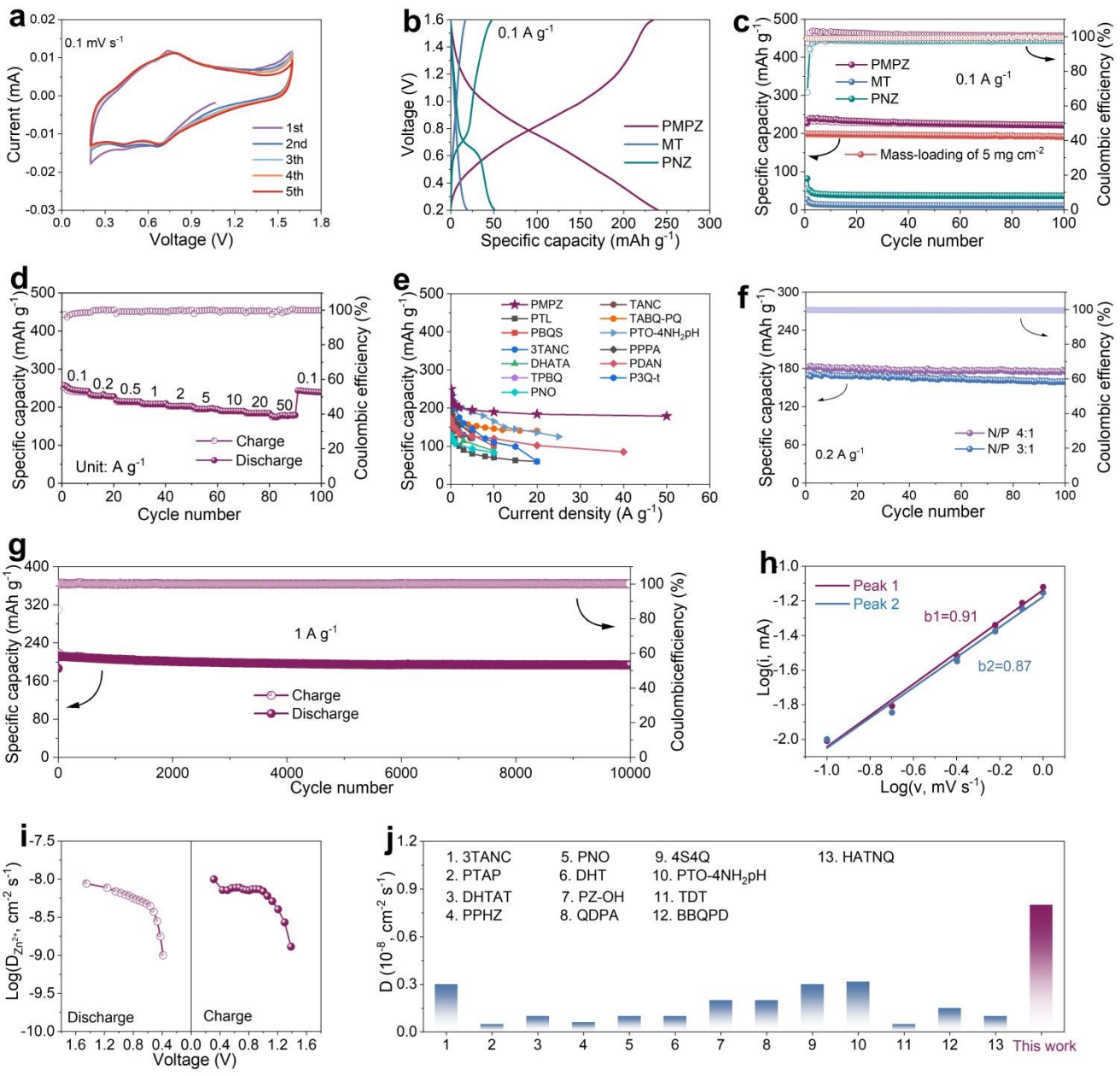

Figure 3. Electrochemical performance of the PMPZ cathodes for AZIBs. (a) CV curves of PMPZ at 0.1 mV s^{-1}. (b) Charge/discharge curves of PMPZ, MT, and PNZ at 0.1 A g^{-1}. (c) Cycling performance of PMPZ with low mass loading and high mass-loading of 5 mg cm^{-2}, together with MT, and PNZ at 0.1 A g^{-1}. (d) Rate performance of PMPZ at different current densities. (e) Rate performance comparison between PMPZ and other reported organic cathodes. (f) Cycling performance of PMPZ with N/P ratios of 3:1 and 4:1 at 0.2 A g^{-1}. (g) Long-term cycling performance of PMPZ at 1 A g^{-1}. (h) The corresponding log (*i*) vs log (*v*) of the PMPZ cathode. (i) Zn^{2+} diffusion coefficients of the PMPZ cathode at different discharge/charge states. (j) Comparison of D_{Zn}^{2+} between PMPZ and various previously reported cathodes.

View Article Online
DOI: 10.1039/D5EE00199H

A g^{-1}, respectively. Upon returning the current density to 0.1 A g^{-1}, the capacity recovered to 239 mAh g^{-1}, illustrating exceptional rate capability and excellent reversibility of PMPZ. Moreover, PMPZ displays similarly shaped charge/discharge curves with minimal voltage polarization across various current densities, confirming rapid reaction kinetics. Importantly, the PMPZ cathode outperforms most reported organic cathodes (**Figure 3e**).[16, 27, 29, 31, 34, 43, 46-51] The excellent rate capability of PMPZ primarily originates from its fully conjugated structure and strong electronegative groups (C=O and C=N), thereby improving the charge transfer and ion storage capability. Furthermore, the Zn//PMPZ pouch cell can power LED lights and keep the LED lights working under bending conditions, highlighting its potential as a viable candidate for advanced electronic devices (**Figure S9**). To better demonstrate the practical application potential of the PMPZ cathode, we further evaluated the Zn//PMPZ cells with N/P ratios of 3:1 and 4:1. As shown in **Figure 3f**, the Zn/PMPZ batteries delivered reversible capacities of 161 and 174 mAh g^{-1} at N/P ratios of 3:1 and 4:1, respectively, after 100 cycles. The excellent performance of PMPZ underscores the advantages of its molecular architecture. Remarkably, the PMPZ cathode demonstrates outstanding long-term cycling stability, delivering a capacity of 194 mAh g^{-1} (91% retention) after 10,000 cycles at 1 A g^{-1} (**Figure 3g**). Notably, PMPZ can maintain well-defined discharge/charge curves at 1 A g^{-1} even after 10,000 cycles (**Figure S8b**). Given its outstanding rate performance, the prolonged cycling performance of PMPZ was further investigated at 20 A g^{-1}. The PMPZ

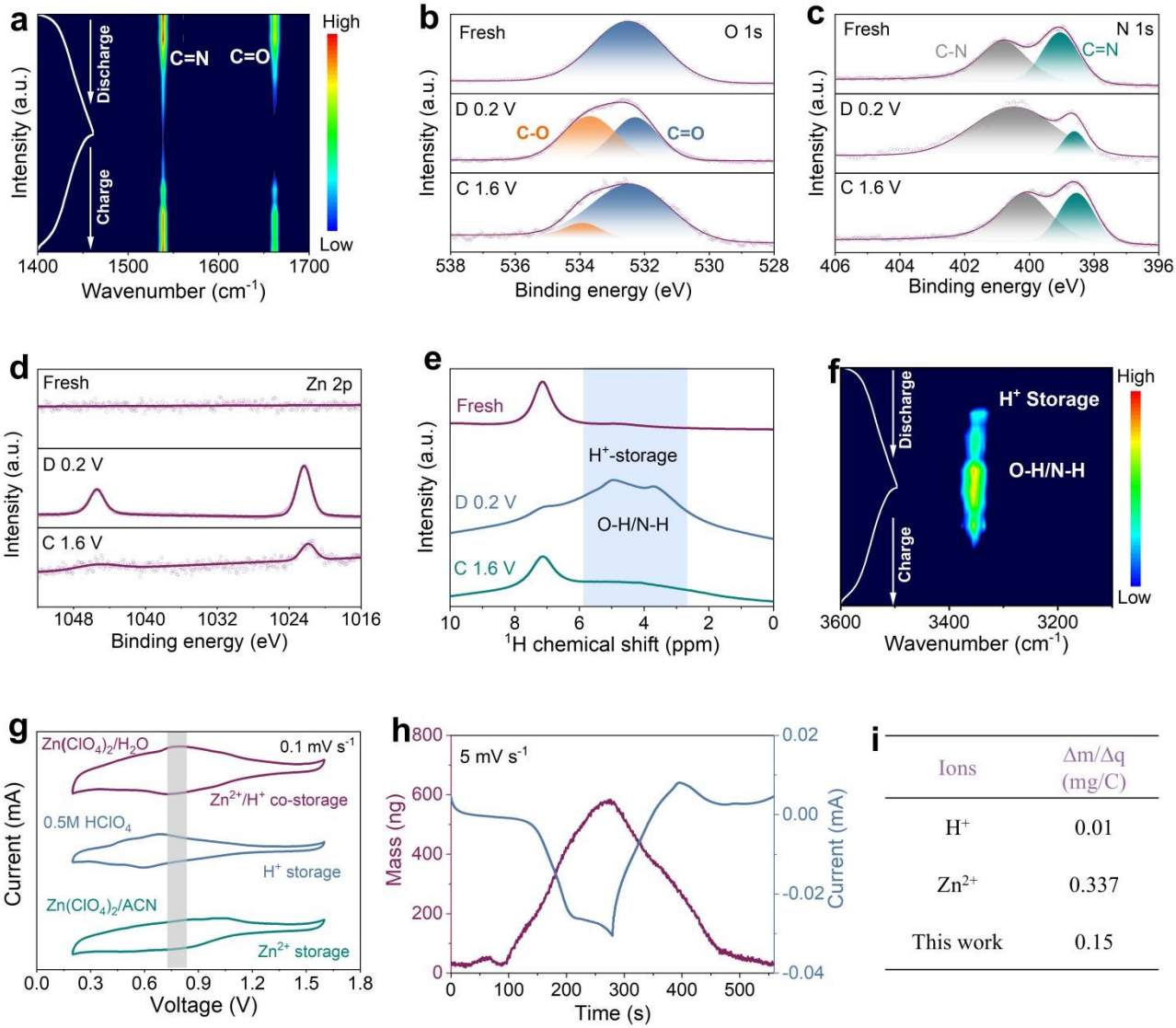

Figure 4. (a) Charge/discharge curves of PMPZ at current density of 0.1 A g^{-1} and operando synchrotron FT-IR spectra of PMPZ during charge/discharge processes. The ex-situ XPS spectra of (b) O 1s, (c) N 1s and (d) Zn 2p of the PMPZ cathode at different charge/discharge states. (e) The ^{1}H SSNMR spectra of the PMPZ cathode at different charge/discharge states. (f) Operando synchrotron FT-IR spectra of PMPZ during charge/discharge processes. (g) CV curves of PMPZ in different electrolytes. (h) Mass change and CV curves of PMPZ in $Zn(ClO_4)_2/H_2O$ electrolyte. (i) The $\Delta m/\Delta q$ of H^+, Zn^{2+}, and PMPZ at 5 mV s^{-1}.

View Article Online DOI: 10.1039/D5EE00192H

cathode demonstrates exceptional cycling stability over 60,000 cycles, maintaining a capacity of 161 mAh g^{-1} with 88% retention (**Figure S10**). Importantly, a single charge/discharge cycle can be completed in approximately one minute, meeting the requirements for ultrafast energy storage. The exceptional cycle performance of PMPZ is primarily attributed to its structural stability enabled by π–π stacking interactions. A comparative analysis with reported organic cathodes for AZIBs further demonstrates the superior performance of PMPZ (**Table S1**).

The CV curves show well-defined reversible redox couples (**Figure S11**) at scan rates ranging from 0.1 to 1 mV s^{-1}, with slight polarization broadening observed at higher scan rates. For the PMPZ cathode, the *b*-values for peaks *b*1 (0.91) and *b*2 (0.87) (**Figure 3h**) are between 0.5 and 1.0. The analysis of the *b*-values reveals that PMPZ exhibits a hybrid charge storage process involving both surface-controlled pseudo-capacitance and diffusion-controlled processes.[40, 52] The Zn^{2+} diffusion coefficients for PMPZ were calculated to be in the range of 10^{-8} ~ 10^{-9} cm^2 s^{-1} (**Figure 3i and S12**). These values exceed those of most reported organic cathodes (**Figure 3j**), indicating superior ion transport kinetics.[27-29, 33, 39, 43, 46, 47, 53-56] The high diffusion coefficients originate from extensive π-conjugated structure of PMPZ, which facilitates electron delocalization and enables efficient charge transfer along polymer chains.[57] In summary, the exceptional electrochemical performance of PMPZ originates from a combination of dominant capacitive contributions, facile ion-insertion kinetics, and highly reversible redox reactions at the cathode.

Charge Storage Mechanism.

The operando synchrotron FT-IR was used to track the dynamic changes of functional groups during the charge/discharge process to elucidate the charge storage mechanism of PMPZ (**Figures 4a**). The pristine material exhibits characteristic vibrational peaks for C=O (1675 cm^{-1}) and C=N (1542 cm^{-1}). During discharging, the intensity of both the C=O and C=N peaks progressively decreased (**Figure 4a**), which is attributed to cations (Zn^{2+} and H^+) coordination with C=O and C=N groups, consuming these active groups.[58, 59] The subsequent charging process fully restored the original spectral features, confirming the high reversibility of this transformation. Additionally, ex-situ XPS analysis further corroborates the storage mechanism during discharging/charging (**Figures 4b-d**). In O 1s spectra (**Figure 4b**), discharging to 0.2 V led to a decrease of the C=O peak intensity (532.2 eV) and the concomitant emergence of a peak at 533.9 eV, which is assigned to C-O species formed via oxygen-cation (Zn^{2+} and H^+) coordination. Upon full charging to 1.6 V, the C=O peak intensity recovered to its initial level, demonstrating its regeneration. Analogous reversible behavior was observed for the nitrogen species (**Figure 4c**). In the N 1s spectra, the discharge process induces a decrease in intensity of the C=N peak (398.5 eV) and a concurrent increase in the C–N peak (401.6 eV), whereas charging results in the opposite evolution, with a reduced C–N peak intensity and a recovered C=N peak intensity. Notably, the N 1s peaks exhibit an overall right shift, which can be ascribed to the increased electron density surrounding nitrogen atoms during charge and discharge process, leading to a binding energy shift of the N 1s peak.[16, 38, 46] Collectively, the FT-IR and XPS results illustrate the reversible redox interconversion between the C=O/C=N and their coordinated counterparts (C-O/C-N). Furthermore, Zn 2p spectra (**Figure 4d**) reveal a significant increase in Zn content at the discharged state and a corresponding decrease upon charging, which directly demonstrates the reversible reaction of Zn^{2+} with the PMPZ polymer.

Notably, aqueous electrolytes containing Zn^{2+} salts (e.g., $Zn(ClO_4)_2$, $Zn(OTF)_2$, $ZnSO_4$) inherently contain significant H^+ concentrations due to unavoidable Zn^{2+} hydrolysis.[60] Therefore, to elucidate the energy storage mechanism of the PMPZ cathode, the involvement of protons (H^+) was investigated in addition to Zn^{2+} storage. Ex-situ ^1H SSNMR was conducted to probe the H^+ storage behavior during electrochemical processes. As displayed in **Figure 4e**, the emergence of new peaks at the 2.0–5.0 ppm region in ^1H SSNMR spectra upon discharging to 0.2 V corresponds to H^+ uptake by the PMPZ electrode, which confirms the insertion of H^+. When the PMPZ cathode was charged back to 1.6 V, the ^1H SSNMR spectra reverted to their original state, demonstrating the high reversibility of H^+ insertion and extraction. Complementary evidence was provided by operando synchrotron FT-IR spectroscopy (**Figure 4f**). Discharge to 0.2 V led to the appearance of new absorption bands in the 3300–3400 cm^{-1} range, characteristic of N–H/O–H stretching vibrations, which results from the protonation of C=N/C=O functional groups. The peak diminished upon charging, reaffirming the reversible nature of H^+ storage. Together, these spectroscopic analyses consistently attest to the reversible co-storage of Zn^{2+} and H^+ in the PMPZ cathode, underscoring its dual-ion charge storage mechanism.

Moreover, to further investigate the contribution of H^+ to charge storage, we analyzed the electrochemical behaviors of PMPZ in distinct electrolytes, including 3M $Zn(ClO_4)_2/H_2O$, 3M $Zn(ClO_4)_2$/ACN, and 0.5M $HClO_4/H_2O$ electrolytes. As shown in CV curves (**Figure 4g)**, PMPZ exhibits similar redox characteristics in both 0.5M $HClO_4/H_2O$ electrolyte (without Zn^{2+}) and 3M $Zn(ClO_4)_2$/ACN electrolyte (without H^+), which is consistent with the behavior observed in 3M $Zn(ClO_4)_2/H_2O$ electrolyte, demonstrating its ability to store both H^+ and Zn^{2+} ions. Crucially, the corresponding charge/discharge curves reveal H^+ storage capacities of 171 mAh g^{-1} in $HClO_4/H_2O$ electrolyte and Zn^{2+} storage capacities of 149 mAh g^{-1} in $Zn(ClO_4)_2$/ACN electrolyte. Both values are significantly lower than the 241 mAh g^{-1} achieved by $Zn(ClO_4)_2/H_2O$ electrolyte containing both ions (Zn^{2+} and H^+) (**Figure S13**). This performance disparity is directly attributable to the absence of the complementary ion in each single-ion system, providing compelling evidence for a synergistic Zn^{2+}/ H^+ co-storage mechanism within the PMPZ cathode.

Then, in-situ electrochemical quartz crystal microbalance with dissipation monitoring (EQCM-D) was employed to track real-time mass and viscoelastic changes in PMPZ cathodes during CV scans (**Figures 4h, S14, and S15**) to further investigate the doping mechanism of PMPZ during redox reaction. During the discharge process, the PMPZ cathode undergoes reduction, absorbing Zn^{2+} and H^+ cations from the electrolyte to maintain charge balance, leading to an increase in mass and a corresponding decrease in frequency (f_3) of the crystal. During the subsequent charge process, PMPZ is oxidized, leading to a decrease in cathode mass due to the expulsion of cations and resultant in an increase in f_3. Notably, the dissipation factor (D_3) remained virtually constant throughout the cycle,

indicating minimal viscoelastic changes and preservation of a rigid polymer structure. After a full cycle, both the frequency and dissipation response recover to their initial values, confirming the high reversibility of the cation doping/dedoping processes in the PMPZ cathodes. Moreover, the mass change per charge transfer ($\Delta m/\Delta q$) was computed to determine the process of charge and mass transfer **(Figures 4h, i)**. In the $Zn(ClO_4)_2/H_2O$ electrolyte, the calculated $\Delta m/\Delta q$ is 0.15 mg C^{-1}. This value is significantly lower than the theoretical mass change expected for exclusive Zn^{2+} insertion/extraction (0.337 mg C^{-1}) but higher than that for exclusive H^+ transfer (0.01 mg C^{-1}). This intermediate value provides direct evidence for the concurrent participation of both Zn^{2+} and H^+ ions in the charge storage process, conclusively demonstrating the Zn^{2+}/ H^+ co-storage mechanism in PMPZ.

View Article Online DOI: 10.1039/D5EE00139H

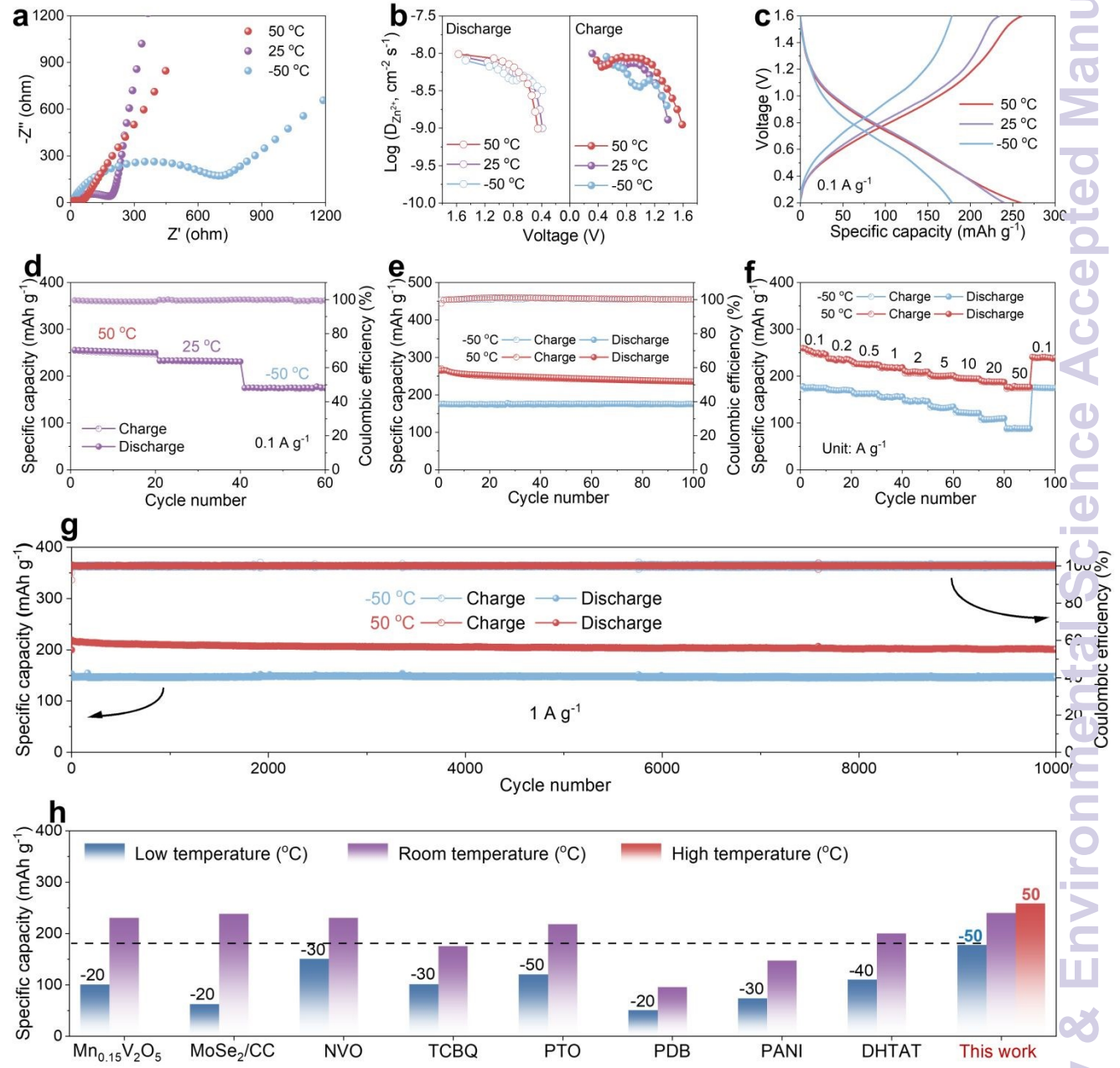

Figure 5. Electrochemical performance of the PMPZ cathode for AZIBs under high and low temperatures. (a) EIS plots of PMPZ at 50, 25, and –50 °C. (b) Zn^{2+} diffusion coefficients of the PMPZ cathode at different temperatures of 50, 25, and –50 °C. (c) Charge/discharge curves of PMPZ at 0.1 A g^{-1} under temperature of 50, 25, and –50 °C. (d) Electrochemical performance of PMPZ across a wide temperature range from –50 to 50 °C. (e) Cycling performance of PMPZ at 0.1 A g^{-1} under temperatures of 50 and –50 °C. (f) Rate performance of PMPZ at different current densities under temperatures of 50 and –50 °C. (g) Long-term cycling performance of PMPZ at 1 A g^{-1} under temperature of 50 and –50 °C. (h) Comparison of specific capacity between PMPZ and previously reported cathode materials under different temperatures.

Electrochemical Performance under Wide Temperature Range

To comprehensively assess the practical applicability and performance advantages of the PMPZ cathode, its electrochemical performance was evaluated across a wide temperature range (50, 25, and −50 °C) in 3 M $Zn(ClO_4)_2$ electrolyte. Prior to low-temperature testing, cathodes were activated by 10 cycles at room temperature (RT).

As shown in **Figure 5a**, In the EIS plots for PMPZ features a semicircle and a subsequent low-frequency Warburg impedance, indicating diffusion through a semi-infinite medium.[1] The linear region in the Nyquist plots indicates the Warburg diffusion impedance (Z_w), reflecting Zn^{2+} diffusion kinetics within the cathode, while the semicircle diameter relates to R_{ct}. Fitting results demonstrate consistently low R_{ct} and Z_w across all temperatures, indicating rapid charge transfer and ion diffusion kinetics with minimal temperature dependence. Notably, although the impedance slightly increases at low temperatures, it still maintains a high charge transfer capacity and a rapid ion diffusion capacity. Then, the Zn^{2+} diffusion coefficients for PMPZ were calculated through GITT measurements to assess its electrochemical kinetics at 50, 25, and −50 °C. As shown in **Figures 5b and S16**, PMPZ maintains a high and consistent ionic diffusion coefficient (10^{-8} ~ 10^{-9} cm^2 s^{-1}) across different temperatures, indicating fast reaction kinetics and strong ion transport capability, and further demonstrating its minimal temperature dependence. This outstanding electrochemical kinetics with low temperature function provides a foundation for developing wide-temperature AZIBs, just as shown in **Figure 5c–h**.

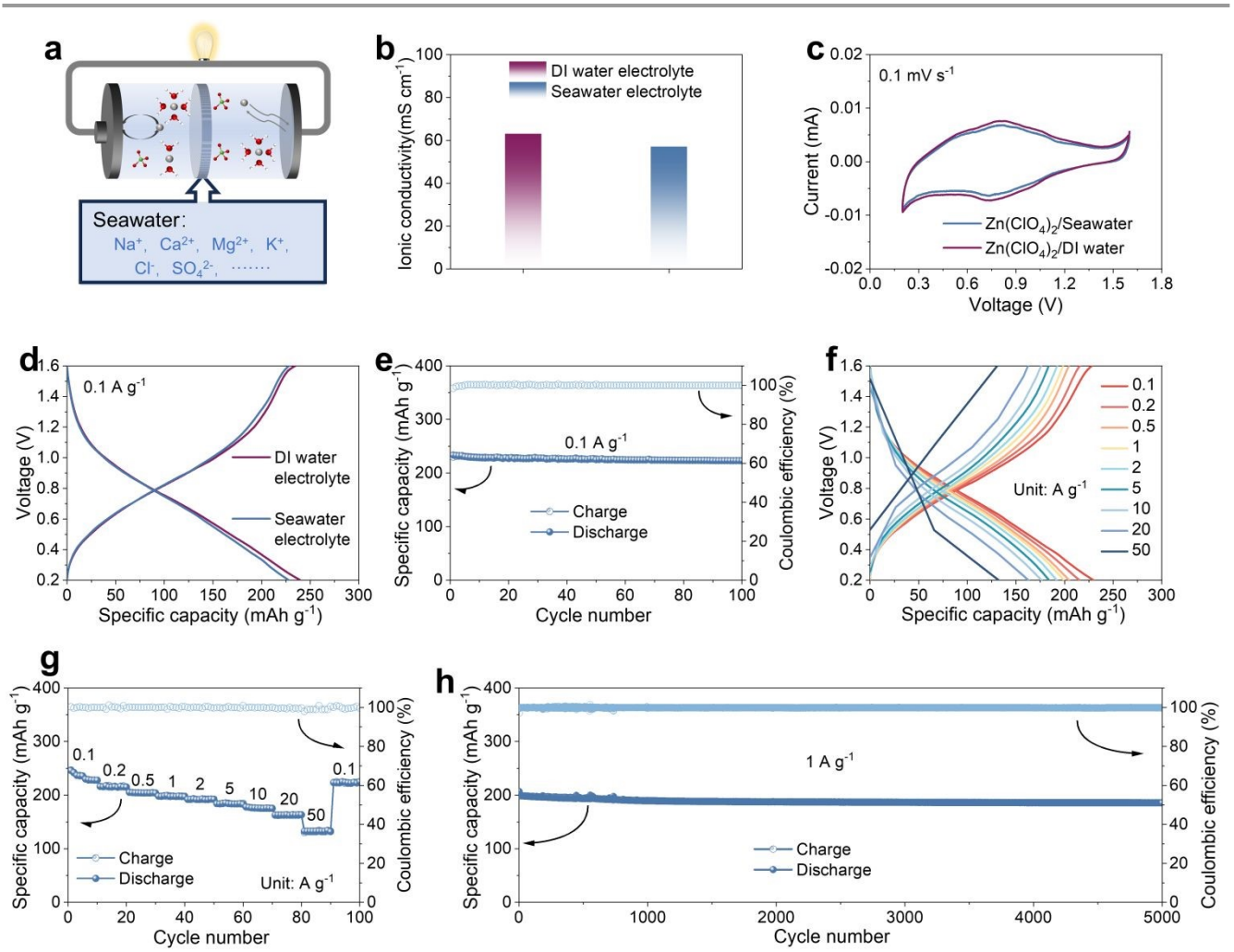

Figure 6. Electrochemical performance of PMPZ with seawater-based electrolyte. (a) Schematic diagram of the Zn//PMPZ cell using seawater-based electrolyte. (b) Ionic conductivity of DI water-based and seawater-based electrolytes (c) CV curves of PMPZ at 0.1 mV s^{-1} with DI water-based and seawater-based electrolytes. (d) Charge/discharge curves of PMPZ at 0.1 A g^{-1} with DI water-based and seawater-based electrolytes. (e) Cycling performance of PMPZ at 0.1 A g^{-1} with seawater-based electrolyte. (f) Charge/discharge curves and (g) rate performance of PMPZ at different current densities with seawater-based electrolyte. (h) Long-term cycling stability of PMPZ at 1 A g^{-1} with seawater-based electrolyte.

View Article Online
DOI: 10.1039/D6EE00199H

The electrochemical performance of the PMPZ cathode was tested at selected temperatures of 50, 25, and –50 °C in 3 M $Zn(ClO_4)_2$ electrolytes. The PMPZ cathode delivers a high discharge capacity of 260 mAh g^{-1} (50 °C) and 175 mAh g^{-1} (−50 °C) at 0.1 A g^{-1} (**Figure 5c, d**), corresponding to 110% and 75% of the discharge capacity achieved at 25 °C (233 mAh g^{-1}), respectively, while maintaining a high coulombic efficiency close to 100% at all tested temperatures. Crucially, PMPZ presents similar charge/discharge curves at high and low temperatures as those at room temperature, without obvious polarization, revealing stable electrochemical kinetics and exceptional adaptability to temperature fluctuations. After that, the cycling stability of the PMPZ cathode was evaluated at 50 and –50 °C. As depicted **Figure 5e and S17**, the PMPZ cathode delivers high reversible discharge capacity of 236 mAh g^{-1} (88% capacity retention) and 175 mAh g^{-1} (99% capacity retention) at 0.1 A g^{-1} after 100 cycles under 50 °C and –50 °C, respectively. Moreover, the PMPZ cathode exhibits attractive rate performance at low and high temperature in the current range 0.1 to 20 A g^{-1} (**Figure 5f**). At 50 °C, capacities values were 258, 238, 223, 218, 209, 200, 195, 188, and 177 mAh g^{-1} at 0.1, 0.2, 0.5, 1, 2, 5, 10, 20. and 50 A g^{-1}, respectively. Importantly, even at low temperature (–50 °C), PMPZ still present remarkable rate performance, with high discharge capacities of 176, 170, 163, 156, 148, 133, 122, 109, and 88 mAh g^{-1} at same current density conditions. Compared with the capacities at 25 °C, the capacity retention values at −50 °C are between 50% and 80%, indicating outstanding capacity retention at low temperature. When the current density returned to 0.1 A g^{-1} from 50 A g^{-1}, the capacity recovered to 241 and 175 mAh g^{-1} at 50 °C and –50 °C, respectively, further confirming excellent stability and reversibility of the PMPZ cathodes at different temperatures. Subsequently, the long-term cycling stability of PMPZ cathodes at 1 A g^{-1} under selected working temperature was evaluated, as shown in **Figure 5g.** The PMPZ cathode reveals remarkable cycling stability at 50 and –50 °C, with a high capacity of 202 mAh g^{-1} (92% capacity retention) at 50 °C and an impressive capacity of 146 mAh g^{-1} (99% capacity retention) at –50 °C after 10000 cycles. The excellent cycling stability mainly results from the extended aromatic backbone and strong intermolecular π-π interaction within the PMPZ polymer. Collectively, these results demonstrate that PMPZ exhibits superior wide-temperature performance, significantly surpassing most reported cathodes (summarized comparatively in **Figure 5h**). The outstanding capacity retention, rate performance, cycling stability, and minimal polarization across an extreme temperature range (−50 °C to 50 °C) unequivocally highlight the practicality and superiority of the PMPZ cathode for AZIBs.

Electrochemical performance under seawater electrolyte

The properties of natural seawater, including its abundance, eco-benignity, and negligible cost, make it an ideal electrolyte for aqueous batteries. Thus, we explored the application of seawater-based electrolytes (3M $Zn(ClO_4)_2$) in AZIBs (**Figure 6a**). Compared to traditional deionized (DI) water-based electrolytes, seawater-based electrolytes exhibit similar high ionic conductivity (**Figure 6b and S18**), which can ensure its fast reaction kinetics. However, the presence of multiple ions (Na^+, Ca^{2+}, Mg^{2+}, K^+, Cl^-, SO_4^{2-}, etc.) in seawater often leads to severe interference, causing most cathodes unsuitable for applications. Therefore, developing high-performance cathode materials capable of operating in complex seawater environments remains a challenge.

The PMPZ cathode enables reversible co-insertion of multivalent and multiple ions (Zn^{2+}/H^+), demonstrating exceptional adaptability to various ionic species. When tested in a seawater-based electrolyte, the PMPZ cathode exhibits the same redox peaks and charge/discharge curves as observed in the DI water-based electrolyte (**Figure 6c, d**), indicating that the complex composition of seawater does not affect the redox behavior of PMPZ. Furthermore, the Zn//PMPZ cell using $Zn(ClO_4)_2$/seawater electrolyte exhibits a high reversible capacity of 223 mAh g^{-1} after 100 cycles at 0.1 A g^{-1}. Moreover, the PMPZ cathode demonstrates remarkable rate performance, with capacities of 230, 216, 204, 197, 192, 183, 175, 162, and 133 mAh g^{-1} at current densities of 0.1, 0.2, 0.5, 1, 2, 5, 10, 20, and 50 A g^{-1}, respectively (**Figure 6f, g**), while maintaining stable charge/discharge curves at various current densities. Additionally, even after 5000 cycles, the cell retains a reversible capacity of 184 mAh g^{-1} at 1 A g^{-1} (**Figure 6h**). These results highlight its outstanding energy storage performance and strong adaptability to complex seawater environments.

Conclusions

In summary, we successfully synthesized PMPZ through a one-step Friedel–Crafts reaction and employed it as a high-performance cathode for AZIBs. The electrochemical performance optimization was achieved through strategic modulation of electron delocalization and integration of multifunctional active groups within its extended π-conjugated architecture. The heterocyclic conjugated units within the PMPZ polymer facilitate extensive electron delocalization along the molecular backbone, resulting in significantly enhanced electron affinity and electronic conductivity. Additionally, the synergistic effect of multiple C=O and C=N groups enable efficient multi-electron redox processes via electron delocalization, markedly elevating the charge storage capability and reaction kinetics at different temperatures. Moreover, integrated theoretical calculation and advanced characterization, including *Operando* synchrotron spectroscopy, EQCM-D, and ex-situ XPS, collectively verify a reversible Zn^{2+}/H^+ co-insertion mechanism involving multi-electron transfer within this conjugated molecular system. Leveraging these synergistic advantages, the PMPZ cathode exhibits high capacity of 240 mAh g^{-1} at 0.1 A g^{-1}, cycling stability beyond 60,000 cycles, and remarkable rate performance of 179 mAh g^{-1} at 50 A g^{-1}, even at seawater electrolyte. Notably, it maintains operational stabilization across extreme temperatures, delivering discharge capacities of 260 mAh g^{-1} at 50°C and 175 mAh g^{-1} at −50 °C under the current density of 0.1 A g^{-1}, with stable cycling exceeding 10,000 cycles at both conditions. Even in seawater-based electrolyte, the PMPZ cathode exhibits high capacity of 223 mAh g^{-1} at 0.1 A g^{-1} and maintains stable performance over 5000 cycles. This work demonstrates a molecular engineering strategy for developing high-performance organic cathode materials

capable of achieving ultra-stable and high-rate AZIBs under harsh operating conditions.

Author contributions

Q. Ma and C. Ji contributed equally to this work. C.Z. and D.C. conceived the idea and designed the experiments. Q.M. and C. Ji conducted the materials characterization and electrochemical measurements. Y.X.., Z.W., L.Z., and R.W. assisted with the electrochemical measurements and data analysis. H.L. conducted the DFT calculations. Q.Z. commented on the paper. Q. M. and C.Z. co-wrote the manuscript. All authors discussed and analyzed the results.

Conflicts of interest

The authors declare no conflict of interest.

Data availability

The data supporting this article have been included as part of the ESI.

Acknowledgements

This work is supported by the National Key R&D Project (2024YFE0101100), under its Singapore-China Joint Flagship Project (Clean Energy), the National Natural Science Foundation of China (U24A2060, 52172173, 52302205), and the Excellent Research and Innovation Team Project of Anhui Province (2022AH010001), the Fundamental Research Funds for the Central Universities (20720250005), Science and Technology Commission of Shanghai Municipality (25DZ3002901, 2024ZDSYS02, 25PY2600100). The authors also acknowledge Anhui Postdoctoral Scientific Research Program Foundation (2025A1029), Postdoctoral Fellowship Program of CPSF under Grant (GZC20250098), China Postdoctoral Science Foundation (2025M770135) and China Postdoctoral Science Foundation-Anhui Joint Support Program (2024T013AH). We also thank the infrared spectroscopy and micro spectroscopy beamline (BL01B) of National Synchrotron Radiation Laboratory (NSRL) for help in characterizations.

References

1. K. Hua, Q. Ma, Y. Liu, P. Xiong, R. Wang, L. Yuan, J. Hao, L. Zhang and C. Zhang, *ACS Nano*, 2025, **19**, 14249-14261.
2. X. Zhang, R. Wang, Z. Liu, Q. Ma, H. Li, Y. Liu, J. Hao, S. Zhang, J. Mao and C. Zhang, *Adv. Energy Mater.*, 2024, **14**, 2400314.
3. C. Zhang, S. Chou, Z. Guo and S. X. Dou, *Adv. Funct. Mater.*, 2024, **34**, 2308001.
4. Z. Mao, H. Wang, T. Zhang, Y. Wang, W. Zhou and D. Chao, *J. Am. Chem. Soc.*, 2025, **147**, 34059-34069.
5. R. Wang, Y. Liu, Q. Luo, P. Xiong, X. Xie, K. Zhou, W. Zhang, L. Zhang, H. J. Fan and C. Zhang, *Adv. Mater.*, 2025, **37**, 2419502.
6. Y. Liu, L. Zhang, L. Liu, Q. Ma, R. Wang, P. Xiong, H. Li, S. Zhang, J. Hao and C. Zhang, *Adv. Mater.*, 2025, **37**, 2415979.
7. Y. Liu, F. Li, J. Hao, H. Li, S. Zhang, J. Mao, T. Zhou, R. Wang, L. Zhang and C. Zhang, *Adv. Funct. Mater.*, 2024, **34**, 2400517.
8. R. Wang, Q. Ma, L. Zhang, Z. Liu, J. Wan, J. Mao, H. Li, S. Zhang, J. Hao, L. Zhang and C. Zhang, *Adv. Energy Mater.*, 2023, **13**, 2302543.
9. W. Zhang, Y. Liu, X. Luo, R. Wang, K. Zhou, L. Yuan, F. Li, H. Li, L. Zhang and C. Zhang, *Adv. Funct. Mater.*, 2025, **35**, e12633.
10. W. Zhou, M. Song, P. Liang, X. Li, X. Liu, H. Li, T. Zhang, B. Wang, R. Zhao, Z. Zhao, W. Li, D. Zhao and D. Chao, *J. Am. Chem. Soc.*, 2023, **145**, 10880-10889.
11. R. Wang, S. Xin, D. Chao, Z. Liu, J. Wan, P. Xiong, Q. Luo, K. Hua, J. Hao and C. Zhang, *Adv. Funct. Mater.*, 2022, **32**, 2207751.
12. X. Luo, L. Jiao, D. Chao, F. Li, R. Wang, S. Zhang, Q. Ma, H. Li, L. Zhang and C. Zhang, *Angew. Chem. Int. Ed.*, 2025, **64**, e202514375.
13. J. Zhu, Q. Zhou, L. Wang, W. Zhou, M. Chen, X. Liu, D. Gao and D. Chao, *Adv. Energy Mater.*, 2024, **14**, 2304554.
14. X. Xie, R. Wang, L. Jiao, H. Li, L. Yuan, S. Zhang, J. Mao and C. Zhang, *Sci. China Chem.*, 2026, DOI: 10.1007/s11426-025-3093-8.
15. H. Jin, D. Zhao and D. Chao, *Joule*, 2025, **9**, 101917.
16. L. Zhao, Y. Jia, Y. Wu, T. Gu, X. Zhou, X. Wang, L. Zhong, S. Zhan, H. Lv, C. Zhi and J. Liu, *Angew. Chem. Int. Ed.*, 2025, **64**, e202425082.
17. Z. Song, L. Miao, H. Duan, Y. Lv, L. Gan and M. Liu, *Angew. Chem. Int. Ed.*, 2024, **63**, e202401049.
18. H. Li, M. Cao, R. Wang, P. Xiong, Y. Liu, L. Zhang, L. Zhang, L. Zhang, D. Chao and C. Zhang, *Angew. Chem. Int. Ed.*, 2025, **64**, e202508057.
19. G. Yang, Y. Zhu, Q. Zhao, Z. Hao, Y. Lu, Q. Zhao and J. Chen, *Sci. China Chem.*, 2023, **67**, 137-164.
20. Y. Wang, W. Zhang, J. Yang, Y. Gong, J. Zhang, M. Fang, Q.-H. Yang and Z. Li, *Matter*, 2022, **5**, 4467-4479.
21. X. Chen, Y. Ma, Y. Lu, H. Zhang, B. Yang and Q. Liu, *Chin. Chem. Lett.*, 2026, **37**, 110666.
22. W. Wang, S. Zhang, L. Zhang, R. Wang, Q. Ma, H. Li, J. Hao, T. Zhou, J. Mao and C. Zhang, *Adv. Mater.*, 2024, **36**, 2400642.
23. L. Zhang, R. Wang, Z. Liu, J. Wan, S. Zhang, S. Wang, K. Hua, X. Liu, X. Zhou, X. Luo, X. Zhang, M. Cao, H. Kang, C. Zhang and Z. Guo, *Adv. Mater.*, 2023, **35**, 2210082.
24. Q. Q. Sun, T. Sun, J. Y. Du, K. Li, H. M. Xie, G. Huang and X. B. Zhang, *Adv. Mater.*, 2023, **35**, 2301088.
25. Z. Li, J. Tan, Y. Wang, C. Gao, Y. Wang, M. Ye and J. Shen, *Energy Environ. Sci.*, 2023, **16**, 2398-2431.
26. T. Chen, Y. Zou, Y. Xu, P. Chen, S. Zeng, K. Hua, H. Liu, Y. Zhou, L. Zhang and C. Zhang, *Chin. Chem. Lett.*, 2025, 111869.
27. R. Wang, Y. Zhang, C. Ma, X. Wang, M. Cai, H. Du, Z. Yang, D. Chao and Y. Wang, *Adv. Funct. Mater.*, 2025, **35**, 2505318.
28. S. Tang, C. Ye and X. Zhou, *Angew. Chem. Int. Ed.*, 2025, **64**, e202501743.
29. W. Li, H. Xu, H. Zhang, F. Wei, L. Huang, S. Ke, J. Fu, C. Jing, J. Cheng and S. Liu, *Nat. Commun.*, 2023, **14**, 5235.
30. P. Bao, L. Cheng, X. Yan, X. Nie, X. Su, H. G. Wang and L.

Chen, *Angew. Chem. Int. Ed.*, 2024, **63**, e202405168.
31. T. Sun, W. Zhang, Z. Zha, M. Cheng, D. Li and Z. Tao, *Energy Storage Mater.*, 2023, **59**, 102778.
32. X. Peng, A. Baktash, N. Alghamdi, M. M. Rana, Y. Huang, X. Hu, C. He, Z. Luo, J. Ning, L. Wang and B. Luo, *Adv. Energy Mater.*, 2024, **14**, 2400147.
33. L. Lin, Z. Lin, J. Zhu, K. Wang, W. Wu, T. Qiu and X. Sun, *Energy Environ. Sci.*, 2023, **16**, 89-96.
34. F. Ye, Q. Liu, H. Dong, K. Guan, Z. Chen, N. Ju and L. Hu, *Angew. Chem. Int. Ed.*, 2022, **61**, e202214244.
35. K. Zhou, H. Yan, Q. Tang, Z. Luo, X. Wang and F. Cai, *J. Power Sources*, 2024, **591**, 233854.
36. L. Zhong, C. Liu, Y. Zhang, J. Li, F. Yang, Z. Zhang and D. Yu, *Angew. Chem. Int. Ed.*, 2024, **64**, e202413971.
37. L. Zhong, C. Wang, J. He, Z. Lin, X. Yang, R. Li, S. Zhan, L. Zhao, D. Wu, H. Chen, Z. Tang, C. ZHi and H. Lv *Adv. Mater.*, 2024, **36**, 2314050.
38. J. Wang, X. Zhang, Z. Liu, J. Yu, H. G. Wang, X. L. Wu, F. Cui and G. Zhu, *Angew. Chem. Int. Ed.*, 2024, **63**, e202401559.
39. R. Wang, J. He, C. Yan, R. Jing, Y. Zhao, J. Yang, M. Shi and X. Yan, *Adv. Mater.*, 2024, **36**, 2402681.
40. Y. Zhang, Q. Huang, Z. Song, L. Miao, Y. Lv, L. Gan and M. Liu, *Adv. Funct. Mater.*, 2024, **35**, 2416415.
41. T. Sun, Z. Yi, W. Zhang, Q. Nian, H. J. Fan and Z. Tao, *Adv. Funct. Mater.*, 2023, **33**, 2306675.
42. X. Liu, J. Tang, D. Bin, Y. Wang, C. Li, L. Su, Y. Shen, W. Hu, Z. Hu, W. Zhuang, B. Yang, H. Lu and Y. Wang, *Energy Storage Mater.*, 2025, **81**, 104517.
43. T. Sun, W. Zhang, Q. Nian and Z. Tao, *Chem. Eng. J.*, 2023, **452**, 139324.
44. T. Chen, H. Banda, L. Yang, J. Li, Y. Zhang, R. Parenti and M. Dincă, *Joule*, 2023, **7**, 986-1002.
45. H. Dai, L. Guan, M. Mao and C. Wang, *Nat. Rev. Clean Technol.*, 2025, **1**, 493-510.
46. Y. Zhang, M. Li, Z. Li, Y. Lu, H. Li, J. Liang, X. Hu, L. Zhang, K. Ding, Q. Xu, H. Liu and Y. Wang, *Angew. Chem. Int. Ed.*, 2024, **63**, e202410342.
47. J. Ning, X. Zhang, D. Xie, Q. He, J. Hu, J. Tang, R. Li, H. Meng and K. X. Yao, *Angew. Chem. Int. Ed.*, 2024, **63**, e202319796.
48. D. Du, J. Zhou, Z. Yin, G. Feng, W. Ji, H. Huang and S. Pang, *Adv. Energy Mater.*, 2024, **14**, 2400580.
49. L. Yan, Q. Zhu, Y. Qi, J. Xu, Y. Peng, J. Shu, J. Ma and Y. Wang, *Angew. Chem. Int. Ed.*, 2022, **61**, e202211107.
50. X. Wang, J. Tang and W. Tang, *Adv. Funct. Mater.*, 2022, **32**, 2200517.
51. X. Yu, K. Zhou, C. Liu, J. Li, J. Ma, L. Yan, Z. Guo and Y. Wang, *Angew. Chem. Int. Ed.*, 2025, **64**, e202501359.
52. Z. Yang, P. Meng, M. Jiang, X. Zhang, J. Zhang and C. Fu, *Angew. Chem. Int. Ed.*, 2024, **63**, e202403424.
53. C. Ding, Y. Zhao, W. Yin, F. Kang, W. Huang and Q. Zhang, *Angew. Chem. Int. Ed.*, 2024, **64**, e202417988.
54. H. Cui, D. Zhang, Z. Wu, J. Zhu, P. Li, C. Li, Y. Hou, R. Zhang, X. Wang, X. Jin, S. Bai and C. Zhi, *Energy Environ. Sci.*, 2024, **17**, 114-122.
55. J. Yang, H. Hua, H. Yang, P. Lai, M. Zhang, Z. Lv, Z. Wen, C. C. Li, J. Zhao and Y. Yang, *Adv. Energy Mater.*, 2023, **13**, 2204005.
56. Y. Chen, J. Li, Q. Zhu, K. Fan, Y. Cao, G. Zhang, C. Zhang, Y. Gao, J. Zou, T. Zhai and C. Wang, *Angew. Chem. Int. Ed.*, 2022, **61**, e202116289.
57. H. Li, M. Cao, Z. Fu, Q. Ma, L. Zhang, R. Wang, F. Liang, T. Zhou and C. Zhang, *Chem. Sci.*, 2024, **15**, 4341-4348.
58. D. Wang, M. Qin, C. Zhang, M. Li, C. Peng, C. Zhi, Q. Li and L. Zhu, *Chem. Sci.*, 2025, **16**, 3630-3637.
59. L. Zhang, Y. Zhang, X. Wang, X. Wang, Q. Wang, J. Li, Z. Li, K. Ding, Y. Peng, H. Liu and Y. Wang, *Adv. Funct. Mater.*, 2025, **36**, e13189.
60. J. Hao, S. Zhang, H. Wu, L. Yuan, K. Davey and S.-Z. Qiao, *Chem. Soc. Rev.*, 2024, **53**, 4312-4332.

View Article Online
DOI: 10.1039/D6EE00199H

Data availability

The data supporting this article have been included as part of the ESI.